HHS Public Access

Author manuscript

Neurobiol Dis. Author manuscript; available in PMC 2021 September 01.

Published in final edited form as:

Neurobiol Dis. 2020 September ; 143: 105016. doi:10.1016/j.nbd.2020.105016.

Modeling UBQLN2-mediated neurodegenerative disease in mice: shared and divergent properties of wild type and mutant UBQLN2 in phase separation, subcellular localization, altered proteostasis pathways, and selective cytotoxicity

Lisa M. Sharkey[1,*], **Stephanie S. Sandoval-Pistorius**[1,2], **Shannon J. Moore**[3], **Julia E. Gerson**[1], **Robert Komlo**[1], **Svetlana Fischer**[1], **Keyshla Y. Negron-Rios**[1], **Emily V. Crowley**[1], **Francisco Padron**[1], **Ronak Patel**[1], **Geoffrey G. Murphy**[3], **Henry L. Paulson**[1,*]

[1]Department of Neurology, University of Michigan, Ann Arbor, MI 48109-2200

[2]Neuroscience Graduate Program, University of Michigan, Ann Arbor, MI 48109

[3]Michigan Neuroscience Institute and Department of Physiology, University of Michigan, Ann Arbor, MI 48109-2200

Abstract

The ubiquitin-binding proteasomal shuttle protein UBQLN2 is implicated in common neurodegenerative disorders due to its accumulation in disease-specific aggregates and, when mutated, directly causes familial frontotemporal dementia/amyotrophic lateral sclerosis (FTD/ALS). Like other proteins linked to FTD/ALS, UBQLN2 undergoes phase separation to form condensates. The relationship of UBQLN2 phase separation and accumulation to neurodegeneration, however, remains uncertain. Employing biochemical, neuropathological and behavioral assays, we studied the impact of overexpressing WT or mutant UBQLN2 in the CNS of transgenic mice. Expression of UBQLN2 harboring a pathogenic mutation (P506T) elicited

[*]To whom correspondence should be addressed: Lisa Sharkey: Department of Neurology, University of Michigan, Ann Arbor, MI 48109-2200; lisams@umich.edu; Tel. (734) 763-3496; Fax (734) 763-3496, Henry Paulson: Department of Neurology, University of Michigan, Ann Arbor, MI 48109-2200; henryp@med.umich.edu; Tel. (734) 615-5632; Fax. (734) 615-5655.

CRediT roles

Lisa M. Sharkey: Conceptualization; Data curation; Formal analysis; Funding acquisition; Investigation; Methodology; Supervision; Validation; Visualization; Writing - original draft.

Stephanie S. Sandoval-Pistorius: Data curation; Investigation; Methodology; Supervision; Validation; Visualization; Roles/Writing - original draft

Shannon J. Moore: Conceptualization; Methodology; Formal analysis; Supervision; Writing - review & editing.

Julia E. Gerson: Investigation; Methodology; Formal analysis; Visualization; Writing - review & editing.

Rob Komlo: Investigation; Formal analysis

Svetlana Fischer: Investigation; Formal analysis; Visualization

Keyshla Y. Negron-Rios: Investigation

Emily V. Crowley: Investigation

Francisco Padron: Data curation

Ronak Patel: Investigation

Geoffrey G. Murphy: Conceptualization; Resources; Software; Writing - review & editing.

Henry L. Paulson: Conceptualization; Funding acquisition; Supervision; Project administration; Resources; Writing - review & editing.

profound and widespread intraneuronal inclusion formation and aggregation without prominent neurodegenerative or behavioral changes. Both WT and mutant UBQLN2 formed ubiquitin- and P62-positive inclusions in neurons, supporting the view that UBQLN2 is intrinsically prone to phase separate, with the size, shape and frequency of inclusions depending on expression level and the presence or absence of a pathogenic mutation. Overexpression of WT or mutant UBQLN2 resulted in a dose-dependent decrease in levels of a key interacting chaperone, HSP70, as well as dose-dependent profound degeneration of the retina. We conclude that, at least in mice, robust aggregation of a pathogenic form of UBQLN2 is insufficient to cause neuronal loss recapitulating that of human FTD/ALS. Our results nevertheless support the view that altering the normal cellular balance of UBQLN2, whether wild type or mutant protein, has deleterious effects on cells of the CNS and retina that likely reflect perturbations in ubiquitin-dependent protein homeostasis.

Keywords

Proteostasis; Ubiquilin; Ubiquitin Proteasome System; Amyotrophic Lateral Sclerosis; Frontotemporal Dementia; protein aggregation; neurodegeneration

Introduction

Ubiquilin2 (UBQLN2) accumulates in common neurodegenerative diseases and, when mutated, directly causes neurodegeneration on the FTD/ALS spectrum (1–7). Here we describe transgenic mouse lines expressing wild type (WT) or disease-linked mutant UBQLN2 that were generated to investigate the biology of this ubiquitin-dependent protein quality control protein. UBQLN2 is one member of a family of ubiquitin adaptor proteins that participate broadly in protein quality control. Its best characterized function is helping to maintain protein homeostasis by shuttling ubiquitinated substrates to the proteasome for degradation (8–11), but it has also been implicated in other protein quality control pathways (12–14). Like the other brain-expressed ubiquilins UBQLN1 and UBQLN4, UBQLN2 has a well characterized N-terminal ubiquitin-like domain (UBL), a C-terminal ubiquitin associated domain (UBA) and four centrally placed STI1 motifs. Unique to UBQLN2 is a proline-rich PXX domain upstream of the UBA domain. When mutated, UBQLN2 causes hereditary FTD/ALS associated with TDP43 accumulation (TDP43-FTD/ALS) (1–4, 15) with most pathogenic UBQLN2 mutations being located in or near the PXX domain (16). Even as a normal protein, however, UBQLN2 accumulates in numerous neurodegenerative diseases including TDP43-FTD/ALS, in which it is a robust biomarker of disease caused by the *C9ORF72* hexanucleotide expansion. (17, 18). These properties link UBQLN2 to other neurodegenerative disease proteins such as TDP43 and P62 that similarly accumulate in neurodegenerative diseases both as wild type protein and when mutated.

Also like TDP43 and P62 (19–21), UBQLN2 undergoes liquid-liquid phase separation (LLPS) *in vitro* and *in vivo* (22, 23). LLPS of proteins and nucleic acids is critical for the formation of nuclear and cytosolic membraneless organelles or condensates, including stress granules (24), nucleoli (25, 26), nuclear paraspeckles (27) P-bodies (28) and nuclear proteolytic compartments (29). Membraneless organelles reversibly concentrate components of key cellular functions. In addition to forming condensates (22, 23), UBQLN2 negatively

regulates the dynamics of FUS-containing stress granules (30). We previously demonstrated that UBQLN2 readily undergoes LLPS and that a FTD/ALS-linked mutation, P506T, decreases UBQLN2 mobility within granules and promotes its aggregation (22).

Yet much remains unknown about the normal and pathological behavior of UBQLN2 in the nervous system. While it is clear that UBQLN2 accumulates in protein deposits in various neurodegenerative diseases (18), the ramifications of UBQLN2 protein accumulation and aggregation remain uncertain. To investigate normal UBQLN2 function and UBQLN2-mediated disease, we generated mouse models that overexpress WT-UBQLN2 or mutant UBQLN2 harboring the FTD/ALS-linked P506T mutation (P506T-UBQLN2). As we recently reported (22), P506T-UBQLN2 but not WT-UBQLN2 robustly aggregates and induces mislocalization and aggregation of TDP43 in neurons of these mice, mirroring the neuropathology of human FTD/ALS caused by UBQLN2 mutations. In the current study, we fully describe the pathological and behavioral effects of WT- or P506T-UBQLN2 expression in transgenic mice. Among our goals, we sought to determine whether the robust aggregation of mutant UBQLN2 in transgenic mice is associated with neuronal degeneration, changes in protein quality control pathways, and behavioral deficits characteristic of FTD/ALS.

Several groups have described mouse models of UBQLN2-mediated ALS/FTD but the neuropathological and behavioral phenotypes have varied (31–34). Some differences across models may reflect differing expression levels of transgenic UBQLN2. Accordingly, we assessed both high-expressing and low-expressing WT-UBQLN2 mouse lines together with a P506T-UBQLN2 line that expresses intermediate levels. Our results show that expression of WT- or P506T-UBQLN2 elicits changes in protein homeostasis pathways and induces highly selective cytotoxicity in a dose-dependent manner. Several changes in UBQLN2 aggregation propensity, sequestration and subcellular localization occur only with mutant P506T-UBQLN2, but both WT- and P506T-UBQLN2 proved cytotoxic to photoreceptors in the retina. Together our findings suggest that optimized UBQLN2 function requires careful balance in cellular levels of the protein to facilitate the protein quality control pathways in which it participates.

Results

To study UBQLN2 function in the CNS and UBQLN-mediated neurodegenerative disease, we generated transgenic mouse lines expressing FLAG-tagged wild type (WT) or mutant (P506T) UBQLN2 from the mouse prion promotor. The current studies represent the full behavioral and neuropathological characterization of these mice, some features of which were recently described (22).

We characterized three transgenic lines, two overexpressing WT-UBQLN2 at low or high levels (WT-low and WT-hi lines) and a third overexpressing P506T-UBQLN2 at a level between the two WT lines. In all three lines, FLAG-UBQLN2 is expressed throughout the brain and spinal cord (Fig. 1A). In WT-low mice, UBQLN2 expression is diffuse and mainly cytoplasmic. At higher expression levels (WT-hi), UBQLN2 is still diffusely expressed but also forms small, spherical puncta in the cytoplasm (Fig. 1A, see also Fig. 3D). In contrast,

P506T-UBQLN2 is neither diffuse nor present in small puncta. Instead, P506T-UBQLN2 forms large, irregular cytoplasmic structures that likely represent aggregated protein.

The robust aggregation of P506T-UBQLN2 is not accompanied by overt signs of neurodegeneration, based on the absence of any difference in lateral ventricle volume in each line at 18 months of age. No changes in ventricular volume were seen across genotypes (nonTg:192727 ± 40160; WT-low: 195820 ± 30020; WT-hi: 174602±14757; and P506T: 200776± 54238, P= 0.4419), suggesting that WT or P506T-UBQLN2 overexpression does not induce prominent or global neurodegeneration in mice.

Despite a growing literature it remains unclear whether, in FTD/ALS, mutant UBQLN2 acts through a dominant toxic mechanism tied to aggregation, through a loss of UBQLN2 function mechanism, or some combination (16, 22, 34, 35). A possible contributing factor could be sequestration of WT-UBQLN2 or other brain-expressed ubiquilins into aggregates formed by mutant UBQLN2. Such sequestration would effectively deplete neurons of a soluble pool of functional ubiquilins. Our transgenic lines allowed us to test this possibility since P506T-UBQLN2 but not WT-UBQLN2 accumulates in the insoluble fraction of brain lysates (22). Consistent with sequestration of WT-UBQLN2 as a potential pathogenic contributor, levels of soluble endogenous murine UBQLN2 are indeed depleted only in P506T-UBQLN2 mouse brain (Fig 1B) with a corresponding increase in the insoluble fraction.

UBQLN2 is usually cytoplasmic but under stress conditions has been reported to translocate to the nucleus where it promotes proteasomal degradation of aggregated proteins (34). Intriguingly, in P506T-UBQLN2 mice but not in WT-UBQLN2 mice, we observed redistribution of UBQLN2 to the nuclei of a discrete subset of brain cells: neuroendothelial cells lining the ventricles (Fig 1C) and spinal cord aqueduct (not shown). Neuroendothelial cells may be particularly sensitive to the cellular stress elicited by P506T-UBQLN2 expression, resulting in nuclear translocation of UBQLN2. Less commonly, we also observe nuclear translocation of P506T-UBQLN2 in neurons, particularly in the hippocampus (Figure 1D) but occasionally in the cortex and cerebellum.

We previously showed that P506T-UBQLN2 mice display cytoplasmic mislocalization and aggregation of TDP43 (22), mirroring the human disease (36–39), and other groups have shown abnormal phosphorylation of extra-nuclear aggregates of TDP43 in ALS/FTD patients (40). By Western blot, however, neither WT-UBQLN2 nor P506T-UBQLN2 transgenic mice showed changes in TDP-43 or phospho-TDP43 levels (Fig 1E, F).

UBQLN2 transgenic mice show changes in protein quality control factors

UBQLN2 is known to participate in the UPS. Consistent with this function and with human disease, UBQLN2 puncta and aggregates found in the neurons of WT-hi and P506T mice strongly costain for ubiquitin (Fig 2F). Ubiquitinated proteins migrating as a high molecular weight smear on gels also accumulated in the insoluble fraction of P506T-UBQLN2 mouse brain (Fig 2E).

UBQLN2 function likely extends beyond the UPS, however. Accordingly, we sought to determine whether expression of WT- or P506T-UBQLN2 altered the behavior of key proteins in other protein quality control pathways, including autophagy-linked proteins and chaperones. Levels of the molecular chaperone HSP70, but not HSP40 and HSP90, are significantly decreased in both WT-hi and P506T mice (Fig 2 A,B). Several STI1 domains in UBQLN2 are postulated to bind HSP70, and UBQLN2 aggregates can sequester binding partners including proteasome subunits (22). Thus, we investigated whether aggregated WT- or P506T-UBQLN2 sequesters HSP70, leading to a decrease in soluble HSP70 levels. By Western blot, HSP70 did not redistribute into the insoluble fraction of brain lysates (Fig. 2C). Moreover, by immunofluorescence, HSP70 only rarely co-localized with WT- and P506T-UBQLN2 puncta (Fig. 2D) indicating that sequestration of HSP70 does not explain the HSP70 decrease.

Since UBQLN2 has been implicated in macroautophagy (12–14) we also measured levels of the autophagy markers p62 and LC3 in brain lysates from UBQLN2 transgenic mice. Both were unchanged (Fig 3 A, B), suggesting that autophagy pathways are not significantly altered by overexpression of WT or mutant UBQLN2. However, UBQLN2 puncta and aggregates in neurons of WT-hi and P506T mice do strongly co-localize with P62 (Fig 3C), similar to what we see for ubiquitin (Fig 2F) and characteristic of the neuropathology in human disease brain (41–43). Although UBQLN2 puncta in WT-hi and P506T both stain positively for P62 and ubiquitin, they differ markedly in size and shape. WT-UBQLN2 puncta are mainly small, spherical and uniform in shape whereas P506T-UBQLN2 puncta are often large and irregularly shaped (Fig 3D).

Both as recombinant protein *in vitro* and when overexpressed in cells, UBQLN2 undergoes liquid-liquid phase separation and accumulates in dynamic structures consistent with membraneless organelles or condensates (22, 23). The puncta observed in WT-hi mice are consistent in size and appearance with such membraneless organelles. And yet their size and spherical appearance, coupled with the fact that they also contain ubiquitin and p62, raised the possibility that they instead represent autophagosomes. To test this possibility, we crossed UBQLN2 WT-hi mice with GFP/RFP-LC3 mice expressing transgenic LC3 tandem-tagged with GFP and RFP (44). Co-immunofluorescence of brain tissue from this cross showed that anti-FLAG labeled WT-UBQLN2 puncta are not positive for GFP/RFP-LC3 (Figure 3E), implying they are not autophagosomes. These results support the view that WT-UBQLN2 puncta in neurons are indeed condensates harboring UBQLN2, ubiquitin and P62.

Overexpression of WT or P506T UBQLN2 does not affect motor behavior in mice

We investigated the effect of expressing WT- or P506T-UBQLN2 on motor performance and other phenotypic measures. Equal numbers of male and female mice from nonTG (n=14), WT-low (n=11) WT-hi (n=13) and P506T (n=15) were evaluated longitudinally at 14, 34, 56 and 83 weeks of age. Weight gain, spontaneous locomotor activity, anxiety-like behavior, motor behavior and vestibular function proved to be similar in all transgenic lines and nonTG control mice. A mixed effects ANOVA was performed for each task with a post-hoc Tukey test used to detect pair-wise differences.

Transgenic mice demonstrated weight curves (Fig 3A) and locomotor and exploratory activities on the open field that were mainly from nonTG mice (Fig 3B,C). Statistical analysis of the open field testing revealed a statistically significant main effect of time (P=0.0002) but not of genotype (P = 0.2275) and no interaction of the factors was detected (P = 0.2908). Analysis of rearing showed a significant main effect of both time (P < 0.0001) and genotype (P = 0.0395) but no interaction effect (P = 0.7440). The ratio of center distance to total distance traveled in the open field test, which provides a measure of anxiety, did not differ between transgenic mice and nonTg mice except for a single measurement in WT-hi mice at 56 weeks (Fig. 3D). Statistical analysis showed a significant main effect time (P = 0.0088) and genotype (0.0024), but no interaction (P = 0.1672). Motor behavior and coordination, measured by time needed to traverse a squared 5-mm beam (Fig 3E) and the latency to fall on the rotarod test (Fig. 3F), did not differ except at 83 weeks of age, when WT-hi mice were slower to cross the balance beam in the first two days of the four-day trial period (Fig 3E). Mixed effects ANOVA of balance beam revealed a main effect of time (P< 0.0001) and genotype (P = 0.0092) and a significant interaction between the factors (P = 0.0391). Mixed effects ANOVA of rotarod showed a significant main effect of time (P < 0.0001) but no main effect of genotype (P = 0.9487) or interaction effect (P = 0.4404).

Behavioral assessment in UBQLN2 mice fails to show cognitive impairment but reveals visual loss in WT-hi mice

To explore the effect of UBQLN2 overexpression on hippocampal-dependent learning, we tested NonTG (n=15), WT-low (n=15), WT-hi (n=13) and P506T (n=9) mice in the standard Morris water maze task (MWM) (45). In the MWM test, mice placed in a pool of opaque water learn to use extra-maze visual clues to locate the position of a platform just below the surface. Mice were trained to find the hidden platform during two sessions per day for 8 days. In each session, mice were placed in the pool and allowed 60 seconds to locate the hidden platform. The latency to find the hidden platform was recorded for each trial, then averaged for each training day. NonTG, WT-low and P506T mice all significantly improved in locating the platform over the 8-day training period, whereas WT-hi mice showed no improvement (Fig 4A). A mixed effects ANOVA revealed statistically significant main effects of both genotype (P < 0.0001) and time (P < 0.0001), as well as an interaction effect (P < 0.0001). A Tukey post-hoc multiple comparison test detected significant differences between WT-hi and nonTG performance at multiple timepoints (Fig 4A).

Approximately 24 hours after the third day of training, and every two days thereafter, mice were tested for their spatial memory of platform location using a 60 sec probe test. During probe tests, the hidden platform was removed and swim paths were analyzed for percent time spent in the quadrant of the pool in which the platform had been previously hidden. Time spent in the target quadrant was then compared to a chance level of 25%. During the first probe test all four mouse strains performed similarly, spending approximately 25% of the time in the platform quadrant (Fig 4B). A mixed effects ANOVA found statistically significant main effects of both genotype (P < 0.0001) and probe number (P < 0.0001), as well as an interaction effect (P = 0.0139). A Post-hoc Tukey multiple comparison test revealed that WT-hi mice performed significantly worse than the other groups on probe trials 2–4 (Fig 2B). In fact, when testing directly against the 25% chance level, WT-hi mice did

not perform statistically better than chance, while all other groups did. Thus, high overexpression of WT-UBQLN2 caused significant impairment in the MWM test, whereas lower level overexpression of WT or mutant UBQLN2 did not lead to significant impairments.

To control for non-cognitive changes that could explain this result, swim speed and time to a visible platform were also measured and analyzed with one-way ANOVA. WT-hi mice performed significantly worse in the visible platform test than nonTG, WT-low or P506T mice (Fig 4D) despite swimming equally well (Fig 4C). This result suggests that the poor performance of the WT-hi mice observed in the MWM were likely due to deficits in visual acuity. Indeed, as described below, WT-hi mice show profound retinal degeneration at 6 months and therefore are unable to use visual cues to learn the platform location.

Because of the visual deficit in WT-hi high mice, we could not use the MWM to fully evaluate the effect of UBQLN2 overexpression on cognitive function. Therefore, we turned to another test of cognitive function routinely employed by our group: fear conditioning (e.g. (46–48)). This task does not require extensive training or invasive preparation, like food or water deprivation, and because both tactile and odor cues are used to differentiate contexts, it relies much less heavily on visual acuity (49). Additionally, by using context-only and cued training paradigms, both hippocampal and non-hippocampal dependent learning can be assessed (50). During Pavlovian fear conditioning, a neutral conditioned stimulus (CS) such as an audible tone or a context, is paired with an aversive unconditioned stimulus (US) such as a foot shock. Upon several pairings of the CS with the US, the animal exhibits a fear response (freezing) when exposed to the CS alone. A lower level of freezing suggests a decreased ability to associate the CS with the US, indicating a learning deficit.

In our study, two CS were utilized: first, a 30 sec audible tone which co-terminated with the foot shock, and second, the context in which the foot shock was administered. During the acquisition phase nonTG (n=10), WT-low (n=11), WT-hi (n=13) and P506T (n=6) mice were exposed to 3 tone-foot shock pairings on each of three successive days. The percent time spent freezing following each foot-shock was measured and averaged daily (Fig 4E). On the fourth day, the animals were placed in the training context without the tone or foot-shock, and the percent time spent freezing was recorded (Fig 4F). A 2-factor repeated measures ANOVA found a significant main effect of time (training days) ($P < 0.0001$) and genotype ($P < 0.0001$) and a significant interaction effect ($P = 0.0411$). Tukey post-hoc tests were performed to determine significant differences between nonTg mice and transgenic mice. All three transgenic lines spent a similar amount of time freezing compared to nonTG mice during both the acquisition stage and the context test (Fig 4E). The next day, the mice were placed in a novel context and their percent time freezing was measured (Fig 4G, pre-tone). The mice were then exposed to the tone (the CS) without foot-shock and the percent freezing time was measured (Fig 4G, tone). A 2-factor repeated measures ANOVA was performed and found a significant main effect of tone (pre vs post-tone) ($P < 0.0001$) and genotype ($P = 0.0139$) and a significant interaction effect ($P = 0.0159$). Sidak post-hoc tests were performed to determine significant differences of transgenic mice from nonTg mice (Fig 4G). As shown in Fig 4H, nonTG, WT-low, and WT-high mice all showed an increase in freezing time post-tone (** = $P < 0.01$). While P506T mice had a similar level of freezing

post-tone as the other strains, the increase in post-tone freezing over pre-tone freezing was not significant.

Discussion

We hypothesized that WT-hi mice developed visual impairment, making it impossible to learn spatial cues in the MWM. To examine this possibility, we dissected eyes from the various mouse lines and evaluated retinal structure by immunofluorescence at 3, 8 and 52 weeks of age (Fig 5A). At 3 weeks of age, all three transgenic lines showed normal retinal structure, similar to nonTG controls. By 8 weeks of age, however, WT-hi mice showed drastic thinning of the retina, losing greater than ~90% of cells in the outer nuclear layer (ONL). In contrast, WT-low and P506T mice maintained normal retinal structure at this time. This retinal degeneration explains why WT-hi mice were unable to use visual spatial clues in the MWM. Retinal degeneration in WT-hi mice is progressive: whereas 8 week old mice still show near-normal thickness of the inner nuclear layer (INL), by 12 months the INL in WT-hi mice is nearly absent.

P506T mice also undergo retinal degeneration albeit more slowly and less completely than WT-hi mice. P506T mice display normal retina structure at 8 weeks, but at 9 months the ONL shows significant thinning (data not shown) and at 12 months the cell loss in the ONL is comparable to that seen in WT-hi mice, yet the INL still appears normal. In contrast, WT-low mice exhibit no appreciable loss to the ONL or INL even at twelve months of age.

Rhodopsin staining of photoreceptors showed normal localization and distribution of rhodopsin at a young age when retina are intact in all transgenic lines (Fig 5A). At 3 weeks of age, when all three transgenic lines have normal retinas, UBQLN2 expression in the retina is consistent with levels seen in the brain (Fig 5C, red). Photoreceptor cells from WT-hi mice contain small, spherical UBQLN2 puncta similar to what is seen in the brain and consistent with phase-separated condensates (Fig 6E). As expected, all three transgenic lines showed higher expression of UBQLN2 than do nonTg mice. Overexpression of UBQLN2 in the retina is highest in the WT-hi mice, intermediate in the P506T mice and lowest in the WT-low line. The data are consistent with UBQLN2-driven retinal degeneration that is dose- and time-dependent.

These results suggest photoreceptors are particularly susceptible to overexpression of UBQLN2. The specialized morphology of photoreceptors and their heavy dependence on protein turnover (51, 52) may make them vulnerable to changes in protein degradation pathways. The rate of retinal degeneration in the WT-hi mice is pronounced between 3 and 8 weeks of age (Fig 5A) suggesting that this critical period of retinal maturation is vulnerable to changes in protein homeostasis. Interestingly, in a recently generated UBQLN2 KO mouse line, the retina at 16 weeks and 12 months (Fig 5B) remains intact, similar to that of nonTG mice. UBQLN2, therefore, is not essential for retinal maturation. Together, our results indicate that high levels of UBQLN2, whether WT or mutant, are toxic to the retina.

The results described here shed light on the behavior of UBQLN2, both as WT and mutant protein, in neurodegenerative disease. Our findings suggest that deleterious effects of P506T-

UBQLN2 in the nervous system are mediated, at least in part, by perturbing the normal propensity of UBQLN2 to engage in LLPS, resulting in aggregation and impaired proteostasis. Some effects are also elicited by high overexpression of WT-UBQLN2, underscoring the importance of careful regulation of cellular UBQLN2 levels in cells of the nervous system.

Consistent with other mouse models expressing mutant UBQLN2 (31) we observed p62- and ubiquitin-positive neuronal inclusions of UBQLN2 throughout the brain and spinal cord, both with WT- and P506T-UBQLN2. Lower levels of WT-UBQLN2 expression in WT-low mice did not lead to visible inclusion formation, indicating that inclusion formation by WT-UBQLN2 is concentration-dependent. The appearance of inclusions, or puncta, differs markedly between WT-hi and P506T mice. In WT-hi mice, UBQLN2 exists both diffusely in the cytoplasm and within small, uniformly spherical puncta that appear to be condensates comprised of UQBLN2 and other molecules linked to protein quality control, including ubiquitin and P62. In contrast, P506T-UBQLN2 exists exclusively in large, irregularly shaped inclusions that are likely aggregates. Recent work describing UBQLN2 LLPS *in vitro* and *in vivo* demonstrated that UBQLN2, like other intrinsically disordered proteins, displays a continuum of mobility in phase-separated granules ranging from liquid droplet to hydrogel and eventually aggregates. The FTD/ALS mutation P506T shifts the spectrum of UBQLN2 mobility toward aggregation, which correlates with neurotoxocity (22). The altered behavior of mutant UBQLN2 mirrors that of TDP-43 in which ALS-linked mutations alter its phase separation dynamics (19, 20, 53) and promote aggregation that is associated with disease (39, 53, 54).

A critical unanswered issue is whether accumulation and aggregation of UBQLN2 is i) central to the neurodegeneration occurring in UBQLN2-linked FTD/ALS, and ii) contributes to the disease process in other neurodegenerative diseases in which WT-UBQLN2 accumulates, such as C9ORF72-linked FTD/ALS. Unfortunately, our models cannot answer this question because we do not observe significant neuronal loss. They do, however, allow us to determine whether the aggregation of mutant UBQLN2 deleteriously sequesters nonmutant ubiquilins, effectively leading to a loss of function. Indeed, expression of aggregation-prone P506T-UBQLN, but not WT-UBQLN, leads to a decrease in soluble murine UBQLN2. This result suggests that when pathogenic forms of UBQLN2 aggregate, they can sequester normal UBQLN2 molecules.

We observed a striking divergence in subcellular localization of WT- versus P506T-UBQLN2 protein in neuroendothelial cells. While transgenic WT-UBQLN2 (like endogenous UBQLN2) is largely cytoplasmic, P506T-UBQLN2 localizes to the nuclei of these cells. Under heat shock or in the presence of aggregated nuclear proteins, UBQLN2 can move to the nucleus (34). Neuroendothelial cells may be particularly sensitive to proteotoxic stress elicited by P506T-UBQLN2, resulting in the observed nuclear localization. Recent work demonstrated that membraneless nuclear organelles including nucleoli and PML bodies are sites of UPS in the nucleus (55, 56), and osmotic stress can drive the formation of intranuclear phase-separated granules thought to be proteolytic compartments (29). UBQLN2's ability to undergo LLPS (22, 23) might allow its incorporation into such nuclear organelles under cellular stress where it would facilitate

ubiquitin-dependent protein degradation. We did not, however, observe P506T-UBQLN2 concentrated within the nucleoli or PML bodies of neuroendothelial cells (data not shown). Nevertheless, it remains possible that phase-separated UBQLN2 condensates in the nucleus are sites of proteasomal degradation. The fact that WT-UBQLN2 localizes to the nucleus under heat shock (34)supports the view that UBQLN2 participates in nuclear protein quality control. Neuroendothelial cells may offer a useful tool with which to explore the factors underlying UBQLN2 translocation to the nucleus.

UBQLN2's best characterized role in protein quality control is in substrate delivery to the UPS, where its interaction with substrates can be facilitated by molecular chaperones such as HSP70. We were therefore intrigued to find that overexpression of P506T- or WT-UBQLN2 led to a decrease in HSP70 levels in brain lysates. Hsp70 levels are unchanged by more modest overexpression of UBQLN2 in WT-low mice, implying that HSP70 reduction is a dose-dependent effect of excess UQBLN2. A potential explanation for this finding is that excess UBQLN2 binds HSP70 via its STI1 domains, thereby promoting HSP70 delivery to the proteasome or another degradation pathway. The implications of decreased hsp70 in UBQLN2-expressing mice have not yet been explored. In principle, increasing the level of UBQLN2 could paradoxically impair handling of substrate proteins whose degradation occurs in a chaperone-dependent manner.

Beyond their role in proteasomal degradation, UBQLN2 and other ubiquilins are also implicated in autophagy. For example, UBQLNs 1 and 2 colocalize with autophagosomes in HeLa cells and mouse tissue (14); and in yeast, the UBQLN homolog Dsk2 promotes autophagic clearance of the Huntington disease protein by facilitating inclusion formation (13). The fact that the spherical UBQLN2 puncta observed in neurons in WT-Hi mice also contain p62 suggests they could represent autophagosomes. Arguing against this possibility is the fact that they do not co-localize with LC3, either by immunofluorescence or when WT-hi mice are crossed to transgenic mice expressing a tandem-tagged GFP/RFP-LC3. We suggest the puncta formed by UBQLN2 are not autophagosomes but instead represent condensates indicative of liquid-liquid-phase separation, as has been described for UBQLN2 *in vitro* (23) and in cell culture (22).

Previous rodent models expressing the human ALS/FTD UBQLN2 mutations P497H (31, 32, 57), P497S (31, 33) or P506T (33, 34) all showed aggregation of mutant UBQLN2 in the CNS, consistent with our observations in P506T-UBQLN2 mice. Overexpressed P497H under control of the endogenous promoter caused dendritic spinopathy, synaptic dysfunction and cognitive impairment without motor deficit (32), while overexpression of P497S and P506T under the Thy1 promoter caused severe motor neuron disease and cognitive changes (33). Viral overexpression of P497H, P497S, and P506T in neonatal mouse brain led to limited and variable motor deficits, and WT overexpression resulted in diffuse staining with small regular puncta (31) similar to our observation in WT-hi mice. Yet despite the robust aggregation of P506T-UBQLN2 throughout the CNS, we do not find evidence to support prominent neurodegeneration or associated motor/behavioral deficits in our transgenic mice. Differences in the promoters used or expression levels may explain discrepancies between our results and previous work. A direct comparison of transgene expression levels across the models would be informative.

Arguably, our most striking finding is the profound retinal degeneration elicited by overexpression of WT-UBQLN2 and, to a lesser extent, P506T-UBQLN2. The retina is known to be sensitive to changes in the activity of protein quality control pathways (58, 59), and many inherited retinopathies are associated with misfolding of specific disease proteins (60). The increased proteotoxic load this places on protein degradation machinery has been suggested to cause retinal cell death (61). The fact that overexpressed UBQLN2 induces robust retinal degeneration, yet mice lacking UBQLN2 show no such retinal loss, favors this being due to a gain of function rather than a loss of function mechanism. As with the decrease in HSP70 levels noted earlier, the retinal degeneration elicited by UBQLN2 is a dose-dependent effect: WT-low mice do not show retinal degeneration. Photoreceptor cells in WT-hi mice contain spherical UBQLN2 puncta, much like neurons in the brain of these same mice, which we suspect are phase-separated condensates. These UBQLN2-rich condensates may serve to concentrate proteasome subunits in a manner that actually induces proteasome insufficiency in photoreceptors. Determining whether perturbation of normal proteasomal function underlies the retinal degeneration caused by UBQLN2 overexpression will require functional readouts of proteasomal activity in the retina.

In summary, overexpression of an FTD/ALS-linked mutant form of UBQLN2 in transgenic mice causes profound and widespread intraneuronal inclusion formation and aggregation without prominent neurodegenerative or behavioral changes. Thus, at least in mice, robust aggregation of a pathogenic form of UBQLN2 appears to be insufficient to cause neuronal loss recapitulating that of human FTD/ALS. Our results nevertheless support the view that altering the normal cellular balance of UBQLN2, whether wild type or mutant protein, has deleterious effects on cells of the CNS. In particular, overexpression of UBQLN2 (WT or P506T) induces a dose-dependent decrease in HSP70 levels and profound retinal degeneration. Our studies in transgenic mice establish that UBQLN2 is intrinsically prone to phase separate in neurons and photoreceptors, manifesting as ubiquitin-positive inclusions that differ in size, shape and frequency depending on the presence or absence of a pathogenic mutation. We speculate that the deleterious properties of overexpressed UBQLN2 are associated with this tendency to phase separate, but the relationship between phase separation, UBQLN2 function in ubiquitin-dependent proteostasis, and its dysfunction in neurodegenerative diseases still requires further study. In addition, future investigations of the mechanisms by which UBQLN2 overexpression induces the rapidly progressive retinal degeneration reported here may decipher the mechanisms by which dysregulation of proteostasis may lead to retinopathies.

Methods

Animals

All animal procedures were approved by the University of Michigan Committee on the Use and Care of Animals and are consistent with the National Institutes of Health guide for the care and use of Laboratory animals (NIH Publications No. 8023, revised 1978). MoPrP-UBQLN2 transgenic mice were generated in a C57BL/6 background strain and genotyped as described previously(22). The UBQLN2 KO mouse was generated by the University of Michigan Transgenic Animal Core using Crispr/Cas9 technology. A single nucleotide

insertion of an adenosine at position 266 in the mouse cDNA sequence results in a premature stop codon 14 basepairs upstream of the insertion site at amino acid position 95 (Fig. S1A). UBQLN2 protein is absent in brain lysate from homozygous knockout mice (Fig S1B). KO mice are genotyped using DNA from mouse tail biopsies by Laragen Inc. (Los Angeles, CA) using a melting curve analysis designed to detect the SNP. This knockout mouse will be more fully described in a future publication. All mice were housed in cages with a maximum number of five animals and maintained in a standard 12-hour light/dark cycle with food and water *ad libitum*.

Tissue harvesting

Animals were deeply anesthetized with ketamine/xylazine mixture and perfused transcardially with 0.1M phosphate buffer. Brains were dissected and divided sagittally. One half was immediately placed on dry ice and stored at − 80°C for biochemical studies while the other half was fixed in 4% paraformaldehyde at 4°C for 48h, and cryoprotected in 30% sucrose in 0.1M phosphate buffer at 4 °C until saturated. Fixed hemispheres were sectioned at 40 μm sagittally through the entire hemisphere using a sledge microtome (SM200R; Leica Biosystems). Free-floating sections were stored at − 20°C for immunostaining. Eyeballs from perfused mice were enucleated and fixed in 4% PFA overnight at 4 degrees. Following fixation, the cornea and the lens were removed to form an eyecup. The eyecup was transitioned through a 10%, 20%, and 30% sucrose gradient. Eyes were embedded in Tissue Plus O.C.T. Compound (Fisher HealthCare, 4585). Eyes were sectioned with a cryostat at 10 um thickness and mounted on Superfrost slides (Fisher Scientific, Pittsburgh, PA).

Immunoblots

Lysates from brain tissue were prepared in RIPA buffer (cat #R0278, Sigma) with protease inhibitors (Roche), PMSF, and PhosphoStop (Roche). Brain tissue was homogenized in a Potter homogenizer, centrifuged (13000 rpm for 30 minutes) and the supernatants were removed. Protein concentration was measured using a BCA assay (cat#23227, ThermoScientific). Samples were prepared in 1x Lamlie sample buffer with DTT, heated at 100°C for 1 min and centrifuged for 1 min at 13000 rpm. Proteins were resolved on 4–12% SDS-polyacrylamide electrophoresis gels and transferred to PVDF membrane, 0.2 um, at 0.35A for 3h at 4°C or for 16h (overnight) at 30V. Membranes were blocked in 5% milk/ 2.5%BSA/TBS-T for 1 hour at RT on a shaker. Primary antibodies were incubated overnight at 4 °C overnight on shaker. Primary antibodies used were: rabbit anti-FLAG (Sigma, cat#F7425) 1:1000, rabbit anti-UBQLN2 1:250 (NBP1–85639, Novus Biologicals) rabbit anti-α-Tubulin 1:10000 (Cell Signaling, cat# 2144) mouse anti-GAPDH (1:5,000, MAB374; Millipore) anti-ubiquitin (Millipore Sigma, MAB1510; 1:500), guinea pig anti-p62 C-terminal (1:200; Progen) Anti-Hsp70 antibody [3A3](Abcam 1:2500), Anti-phospho TDP-43 (Ser409/Ser410) MABN14 (Milipore, 10:1000), anti- TARDBP, 10782–2-AP (ProteinTech, 1:500), anti-HSP40, cat4868 (Cell Signalling, 1:1000), Anti-Hsp90 alpha antibody (ab2928) (Abcam 1:2000) and anti-LC3 pAb PM036 (MBL, 1:10,000). Secondary antibodies were peroxidase-conjugated goat anti-rabbit, goat anti-mouse or goat anti-guinea pig (1:10,000; Jackson Immunoresearch) incubated for 1h at RT on shaker. Blots were developed with enhanced chemiluminescence (ECL)-plus reagent (Western Lighting; PerkinElmer) and exposure to autoradiography films.

Immunofluorescence on brain sections

Brain sections were subjected to a basic antigen retrieval, washed, blocked, and incubated overnight at 4°C in primary antibody supplemented with 0.025% Triton X-100, 0.5% BSA, and 5% serum from the host line for secondary antibodies (donkey or goat). Primary antibodies used in these studies included the following: anti-ubiquitin (Millipore Sigma, MAB1510; 1:500), guinea pig anti-p62 C-terminal (1:200; Progen), rabbit anti-FLAG (Sigma, cat#F7425) 1:1000, rabbit anti-UBQLN2 1:250 (NBP1–85639, Novus Biologicals), anti-N-terminal HTT (1:250; Santa Cruz Biotechnology). Primary incubated sections were then washed and incubated with the corresponding secondary Alexa Fluor 405, 488 or 568 antibodies (1:1,000; Invitrogen). All sections were stained with DAPI (Sigma) for 15 min at room temperature, mounted with Prolong Gold Antifade Reagent (Invitrogen), and imaged using an IX71 Olympus inverted microscope or Olympus confocal microscope.

Immunofluorescence on retina sections

10 um sections from fixed retinas were washed in PBS, permeablized with 0.5% Triton-X followed by 3×10 minute washes in 0.1% Tween20. Sections were then washed with 70% ethanol for 5 mins. Sections were incubated in Autofluorescence Eliminator Reagent (Millipore for 10 minutes) followed by three 1-minute washes and one 5-minute wash in 70% ethanol. Sections were blocked in 5% goat serum for 1 hr at room temperature followed by a 30 minute incubation in goat anti-mouse FAB (1:30). Sections were incubated in primary antibodies (anti-rhodopsin, Abcam, 1:250; Anti-UBQLN2, Novus, 1:350) at 4C overnight. The following day, sections were washed in 0.1% Tween20 three times for 10 minutes and incubated in goat-anti-mouse IgG Alexa Fluor 488 (Invitrogen, 1:500) at room temperature for one hour. Sections were then washed in 0.1% Tween20 3×10 minutes and incubated in DAPI (Sigma) for 15 minutes at room temperature. Sections were then washed in 0.1% Tween20 three times for 10 minutes prior to being cover-slipped with Prolong Gold Antifade Reagent (Invitrogen). Slides were imaged using an Olympus confocal microscope.

Motor phenotyping

UBQLN2 transgenic and control littermates were mice assessed in weight and motor function at 14, 32, 56 and 83 weeks. Motor coordination and balance was tested by assessing the ability of mice to traverse a 5-mm-wide, 44-cm-long Plexiglas square beam from a clear 20 × 20 cm platform to an enclosed black box 20 × 20 × 20 cm, at a 53 cm height. Mice crossed the beam for two trials on each of 4 days of testing. Time to traverse the beam was recorded for each trial with a maximum cutoff of 20 seconds with falls scored as 20 seconds. Rotarod was used as a secondary method to assess motor and vestibular function. Mice were trained for 3 consecutive days on an accelerating rotarod, 4–40rpm for 5 min, two trials per day with a resting interval of 30 min between trials. On Day 4 the mice were tested using two trials of 5 min on the accelerating rod 4–40rpm with a 30-minute rest between trials. The average latency to fall time for the two trials was recorded. Locomotor and exploratory activities were assessed by recording the mice for 30 minutes in a photobeam activity system open-field apparatus (San Diego Instruments, San Diego, CA). Locomotor activity corresponds to the total distance traversed by the mice, which is calculated from the total number of beam breaks. Exploratory activity was measured by the total number of rears. The

ratio of total distance traveled to distance travelled at the periphery of the field was used as a measurement of anxiety-like behavior.

Morris water maze

The Morris water maze (MWM) consisted of a 1.2-meter diameter pool filled with water that was made opaque with white nontoxic paint. Water temperature was maintained at 25 ± 2 C° throughout the experiment.

Every training trial began with the mouse placed on the platform for 15 sec. The mouse was then placed into the water facing the wall of the pool and allowed to search for the platform. The trial ended either when the mouse climbed onto the platform or when 60 sec had elapsed. At the end of each trial, the mouse was allowed to rest on the platform for 15 sec. Mice were given six trials per day for 8 d, with the starting position for each trial chosen pseudorandomly among seven start positions. Probe trials were conducted 24 h after the third training session and every 2 days after that. Probe trials were conducted prior to the days' training sessions. During the probe trial, the escape platform was removed and mice were placed in the pool at the start location directly opposite from where the platform was and allowed to swim for 60 sec. Mice were tested on the visible-platform version of the water maze 24 h following the last probe trial. The visible-platform version consisted of a single day of training with six trials, during which the platform was marked with a distinct visual cue; the platform was moved to a new quadrant (excluding the target quadrant from the hidden-platform version) for each set of two trials.

Fear conditioning

Four conditioning chambers, designed for mice (Med Associates), were arranged in a 2 × 2 configuration on a steel rack in an isolated room. The front, top, and back of the chamber were made of clear acrylic and the two sides made of modular aluminum, and all chambers were lit by white overhead lighting. A stainless steel grid floor was positioned over a stainless-steel drop-pan, which was lightly cleaned with 70% ethyl alcohol to provide a background odor. Each grid was connected to a solid-state shock scrambler and each scrambler was connected to an electronic constant-current shock source that was controlled via an interface connected to a Dell Windows XP computer running Actimetrics FreezeFrame software. Four cameras were mounted (one above each chamber) to the steel rack, and video signals were sent to the same computer. Freezing was assessed using the Actimetrics FreezeFrame software, which digitizes the video signal at 4 Hz and compares movement frame by frame to determine the amount of freezing.

Mice were transferred from their home cages into the conditioning chambers individually in groups of four at one time. On each of 3 consecutive days of conditioning, mice were placed in the chamber for 3 min prior to the onset of tone-shock pairings. The tone-shock pairings consisted of a 30 sec tone (2.8 kHz, 75dB) which co-terminated with a 2-sec, 0.75 mA footshock. Three tone-shock pairings separated by 30 sec were delivered each day. To test contextual memory, 24 hrs after the last training trial, mice were placed in the training context for 5 min in the absence of tone or foot shock and the percentage of time spent freezing was recorded. Twenty-four hours later, to test cued memory, the animals were

placed in a novel environment, which consisted of white acrylic inserts to cover the grid floor and walls, red light, and 2% acetic acid scent; after a 3 min baseline, the 30 sec tone was delivered 3 times with a 30 second inter-stimulus interval and the percent time freezing was recorded.

Supplementary Material

Refer to Web version on PubMed Central for supplementary material.

Acknowledgments

• R21 NS093469-01 NIH/NINDS (Sharkey, Paulson) 07/01/15-6/30/17; *Investigating mechanisms of UBQLN2-mediated neurodegenerative disease*

• 5 R01 NS096785-10 NIH-DHHS-US (Paulson) 02/01/16- 01/01/21; *Integrating Quality Control: Studies of UBQLN2 in Age-Related Neurodegeneration*

• Protein Folding Diseases Initiative; University of Michigan Medical SchoolALS Association; Defining the role of Ubiquilins in ALS/FTD Amyotrophic Lateral Sclerosis

• University of Michigan Transgenic Animal Core; https://brcf.medicine.umich.edu/cores/transgenic-animal-model/

References

1. Deng HX, Chen W, Hong ST, Boycott KM, Gorrie GH, Siddique N, Yang Y, Fecto F, Shi Y, Zhai H, Jiang H, Hirano M, Rampersaud E, Jansen GH, Donkervoort S, Bigio EH, Brooks BR, Ajroud K, Sufit RL, Haines JL, Mugnaini E, Pericak-Vance MA, Siddique T. Mutations in UBQLN2 cause dominant X-linked juvenile and adult-onset ALS and ALS/dementia. Nature. 2011;477(7363):211–5. doi: 10.1038/nature10353.; [PubMed: 21857683]
2. Fahed AC, McDonough B, Gouvion CM, Newell KL, Dure LS, Bebin M, Bick AG, Seidman JG, Harter DH, Seidman CE. UBQLN2 mutation causing heterogeneous X-linked dominant neurodegeneration. Annals of neurology. 2014. doi: 10.1002/ana.24164.
3. Scotter EL, Smyth L, Bailey J, Wong CH, de Majo M, Vance CA, Synek BJ, Turner C, Pereira J, Charleston A, Waldvogel HJ, Curtis MA, Dragunow M, Shaw CE, Smith BN, Faull RLM. C9ORF72 and UBQLN2 mutations are causes of amyotrophic lateral sclerosis in New Zealand: a genetic and pathologic study using banked human brain tissue. Neurobiology of aging. 2017;49:214 e1–e5. doi: 10.1016/j.neurobiolaging.2016.06.019.
4. Williams KL, Warraich ST, Yang S, Solski JA, Fernando R, Rouleau GA, Nicholson GA, Blair IP. UBQLN2/ubiquilin 2 mutation and pathology in familial amyotrophic lateral sclerosis. Neurobiology of aging. 2012;33(10):2527 e3–10. doi: 10.1016/j.neurobiolaging.2012.05.008.
5. Synofzik M, Maetzler W, Grehl T, Prudlo J, Vom Hagen JM, Haack T, Rebassoo P, Munz M, Schols L, Biskup S. Screening in ALS and FTD patients reveals 3 novel UBQLN2 mutations outside the PXX domain and a pure FTD phenotype. Neurobiology of aging. 2012;33(12):2949 e13–7. doi: 10.1016/j.neurobiolaging.2012.07.002.
6. Gellera C, Tiloca C, Del Bo R, Corrado L, Pensato V, Agostini J, Cereda C, Ratti A, Castellotti B, Corti S, Bagarotti A, Cagnin A, Milani P, Gabelli C, Riboldi G, Mazzini L, Soraru G, D'Alfonso S, Taroni F, Comi GP, Ticozzi N, Silani V, Consortium S. Ubiquilin 2 mutations in Italian patients with amyotrophic lateral sclerosis and frontotemporal dementia. Journal of neurology, neurosurgery, and psychiatry. 2013;84(2):183–7. Epub 2012/11/10. doi: 10.1136/jnnp-2012-303433.
7. Daoud H, Suhail H, Szuto A, Camu W, Salachas F, Meininger V, Bouchard JP, Dupre N, Dion PA, Rouleau GA. UBQLN2 mutations are rare in French and French-Canadian amyotrophic lateral sclerosis. Neurobiology of aging. 2012;33(9):2230 e1–e5. Epub 2012/05/09. doi: 10.1016/j.neurobiolaging.2012.03.015.

8. Ko HS, Uehara T, Tsuruma K, Nomura Y. Ubiquilin interacts with ubiquitylated proteins and proteasome through its ubiquitin-associated and ubiquitin-like domains. FEBS letters. 2004;566(1–3):110–4. doi: 10.1016/j.febslet.2004.04.031. [PubMed: 15147878]

9. Elsasser S, Gali RR, Schwickart M, Larsen CN, Leggett DS, Muller B, Feng MT, Tubing F, Dittmar GA, Finley D. Proteasome subunit Rpn1 binds ubiquitin-like protein domains. Nature cell biology. 2002;4(9):725–30. Epub 2002/08/29. doi: 10.1038/ncb845. [PubMed: 12198498]

10. Rao H, Sastry A. Recognition of specific ubiquitin conjugates is important for the proteolytic functions of the ubiquitin-associated domain proteins Dsk2 and Rad23. The Journal of biological chemistry. 2002;277(14):11691–5. Epub 2002/01/24. doi: 10.1074/jbc.M200245200. [PubMed: 11805121]

11. Kleijnen MF, Shih AH, Zhou P, Kumar S, Soccio RE, Kedersha NL, Gill G, Howley PM. The hPLIC proteins may provide a link between the ubiquitination machinery and the proteasome. Molecular cell. 2000;6(2):409–19. [PubMed: 10983987]

12. Senturk M, Lin G, Zuo Z, Mao D, Watson E, Mikos AG, Bellen HJ. Ubiquilins regulate autophagic flux through mTOR signalling and lysosomal acidification. Nature cell biology. 2019;21(3):384–96. Epub 2019/02/26. doi: 10.1038/s41556-019-0281-x.; [PubMed: 30804504]

13. Chuang KH, Liang F, Higgins R, Wang Y. Ubiquilin/Dsk2 promotes inclusion body formation and vacuole (lysosome)-mediated disposal of mutated huntingtin. Molecular biology of the cell. 2016;27(13):2025–36. doi: 10.1091/mbc.E16-01-0026.; [PubMed: 27170182]

14. Rothenberg C, Srinivasan D, Mah L, Kaushik S, Peterhoff CM, Ugolino J, Fang S, Cuervo AM, Nixon RA, Monteiro MJ. Ubiquilin functions in autophagy and is degraded by chaperone-mediated autophagy. Human molecular genetics. 2010;19(16):3219–32. doi: 10.1093/hmg/ddq231.; [PubMed: 20529957]

15. Ling SC, Polymenidou M, Cleveland DW. Converging mechanisms in ALS and FTD: disrupted RNA and protein homeostasis. Neuron. 2013;79(3):416–38. doi: 10.1016/j.neuron.2013.07.033. [PubMed: 23931993]

16. Renaud L, Picher-Martel V, Codron P, Julien JP. Key role of UBQLN2 in pathogenesis of amyotrophic lateral sclerosis and frontotemporal dementia. Acta neuropathologica communications. 2019;7(1):103 Epub 2019/07/20. doi: 10.1186/s40478-019-0758-7.; [PubMed: 31319884]

17. Brettschneider J, Van Deerlin VM, Robinson JL, Kwong L, Lee EB, Ali YO, Safren N, Monteiro MJ, Toledo JB, Elman L, McCluskey L, Irwin DJ, Grossman M, Molina-Porcel L, Lee VM, Trojanowski JQ. Pattern of ubiquilin pathology in ALS and FTLD indicates presence of C9ORF72 hexanucleotide expansion. Acta neuropathologica. 2012;123(6):825–39. doi: 10.1007/s00401-012-0970-z.; [PubMed: 22426854]

18. Mori F, Tanji K, Odagiri S, Toyoshima Y, Yoshida M, Ikeda T, Sasaki H, Kakita A, Takahashi H, Wakabayashi K. Ubiquilin immunoreactivity in cytoplasmic and nuclear inclusions in synucleinopathies, polyglutamine diseases and intranuclear inclusion body disease. Acta neuropathologica. 2012;124(1):149–51. doi: 10.1007/s00401-012-0999-z. [PubMed: 22661321]

19. Conicella AE, Zerze GH, Mittal J, Fawzi NL. ALS Mutations Disrupt Phase Separation Mediated by alpha-Helical Structure in the TDP-43 Low-Complexity C-Terminal Domain. Structure. 2016;24(9):1537–49. Epub 2016/08/23. doi: 10.1016/j.str.2016.07.007.; [PubMed: 27545621]

20. Gopal PP, Nirschl JJ, Klinman E, Holzbaur EL. Amyotrophic lateral sclerosis-linked mutations increase the viscosity of liquid-like TDP-43 RNP granules in neurons. Proceedings of the National Academy of Sciences of the United States of America. 2017;114(12):E2466–E75. Epub 2017/03/08. doi: 10.1073/pnas.1614462114.; [PubMed: 28265061]

21. Sun D, Wu R, Zheng J, Li P, Yu L. Polyubiquitin chain-induced p62 phase separation drives autophagic cargo segregation. Cell Res. 2018;28(4):405–15. Epub 2018/03/07. doi: 10.1038/s41422-018-0017-7.; [PubMed: 29507397]

22. Sharkey LM, Safren N, Pithadia AS, Gerson JE, Dulchavsky M, Fischer S, Patel R, Lantis G, Ashraf N, Kim JH, Meliki A, Minakawa EN, Barmada SJ, Ivanova MI, Paulson HL. Mutant UBQLN2 promotes toxicity by modulating intrinsic self-assembly. Proceedings of the National Academy of Sciences of the United States of America. 2018;115(44):E10495–E504. doi: 10.1073/pnas.1810522115.; [PubMed: 30333186]

23. Dao TP, Kolaitis RM, Kim HJ, O'Donovan K, Martyniak B, Colicino E, Hehnly H, Taylor JP, Castaneda CA. Ubiquitin Modulates Liquid-Liquid Phase Separation of UBQLN2 via Disruption of Multivalent Interactions. Molecular cell. 2018;69(6):965–78 e6. doi: 10.1016/j.molcel.2018.02.004. [PubMed: 29526694]
24. Molliex A, Temirov J, Lee J, Coughlin M, Kanagaraj AP, Kim HJ, Mittag T, Taylor JP. Phase separation by low complexity domains promotes stress granule assembly and drives pathological fibrillization. Cell. 2015;163(1):123–33. doi: 10.1016/j.cell.2015.09.015.; [PubMed: 26406374]
25. Feric M, Vaidya N, Harmon TS, Mitrea DM, Zhu L, Richardson TM, Kriwacki RW, Pappu RV, Brangwynne CP. Coexisting Liquid Phases Underlie Nucleolar Subcompartments. Cell. 2016;165(7):1686–97. Epub 2016/05/24. doi: 10.1016/j.cell.2016.04.047.; [PubMed: 27212236]
26. Nemeth A, Grummt I. Dynamic regulation of nucleolar architecture. Curr Opin Cell Biol. 2018;52:105–11. Epub 2018/03/13. doi: 10.1016/j.ceb.2018.02.013. [PubMed: 29529563]
27. Yamazaki T, Souquere S, Chujo T, Kobelke S, Chong YS, Fox AH, Bond CS, Nakagawa S, Pierron G, Hirose T. Functional Domains of NEAT1 Architectural lncRNA Induce Paraspeckle Assembly through Phase Separation. Molecular cell. 2018;70(6):1038–53 e7. Epub 2018/06/23. doi: 10.1016/j.molcel.2018.05.019. [PubMed: 29932899]
28. Kroschwald S, Maharana S, Mateju D, Malinovska L, Nuske E, Poser I, Richter D, Alberti S. Promiscuous interactions and protein disaggregases determine the material state of stress-inducible RNP granules. eLife. 2015;4:e06807 Epub 2015/08/05. doi: 10.7554/eLife.06807.; [PubMed: 26238190]
29. Yasuda S, Tsuchiya H, Kaiho A, Guo Q, Ikeuchi K, Endo A, Arai N, Ohtake F, Murata S, Inada T, Baumeister W, Fernandez-Busnadiego R, Tanaka K, Saeki Y. Stress- and ubiquitylation-dependent phase separation of the proteasome. Nature. 2020;578(7794):296–300. Epub 2020/02/07. doi: 10.1038/s41586-020-1982-9. [PubMed: 32025036]
30. Alexander EJ, Ghanbari Niaki A, Zhang T, Sarkar J, Liu Y, Nirujogi RS, Pandey A, Myong S, Wang J. Ubiquilin 2 modulates ALS/FTD-linked FUS-RNA complex dynamics and stress granule formation. Proceedings of the National Academy of Sciences of the United States of America. 2018;115(49):E11485–E94. doi: 10.1073/pnas.1811997115.; [PubMed: 30442662]
31. Ceballos-Diaz C, Rosario AM, Park HJ, Chakrabarty P, Sacino A, Cruz PE, Siemienski Z, Lara N, Moran C, Ravelo N, Golde TE, McFarland NR. Viral expression of ALS-linked ubiquilin-2 mutants causes inclusion pathology and behavioral deficits in mice. Molecular neurodegeneration. 2015;10:25. doi: 10.1186/s13024-015-0026-7.; [PubMed: 26152284]
32. Gorrie GH, Fecto F, Radzicki D, Weiss C, Shi Y, Dong H, Zhai H, Fu R, Liu E, Li S, Arrat H, Bigio EH, Disterhoft JF, Martina M, Mugnaini E, Siddique T, Deng HX. Dendritic spinopathy in transgenic mice expressing ALS/dementia-linked mutant UBQLN2. Proceedings of the National Academy of Sciences of the United States of America. 2014. doi: 10.1073/pnas.1405741111.
33. Le NT, Chang L, Kovlyagina I, Georgiou P, Safren N, Braunstein KE, Kvarta MD, Van Dyke AM, LeGates TA, Philips T, Morrison BM, Thompson SM, Puche AC, Gould TD, Rothstein JD, Wong PC, Monteiro MJ. Motor neuron disease, TDP-43 pathology, and memory deficits in mice expressing ALS-FTD-linked UBQLN2 mutations. Proceedings of the National Academy of Sciences of the United States of America. 2016;113(47):E7580–E9. doi: 10.1073/pnas.1608432113.; [PubMed: 27834214]
34. Hjerpe R, Bett JS, Keuss MJ, Solovyova A, McWilliams TG, Johnson C, Sahu I, Varghese J, Wood N, Wightman M, Osborne G, Bates GP, Glickman MH, Trost M, Knebel A, Marchesi F, Kurz T. UBQLN2 Mediates Autophagy-Independent Protein Aggregate Clearance by the Proteasome. Cell. 2016;166(4):935–49. doi: 10.1016/j.cell.2016.07.001.; [PubMed: 27477512]
35. Teyssou E, Chartier L, Amador MD, Lam R, Lautrette G, Nicol M, Machat S, Da Barroca S, Moigneu C, Mairey M, Larmonier T, Saker S, Dussert C, Forlani S, Fontaine B, Seilhean D, Bohl D, Boillee S, Meininger V, Couratier P, Salachas F, Stevanin G, Millecamps S. Novel UBQLN2 mutations linked to amyotrophic lateral sclerosis and atypical hereditary spastic paraplegia phenotype through defective HSP70-mediated proteolysis. Neurobiology of aging. 2017;58:239 e11–e20. Epub 2017/07/19. doi: 10.1016/j.neurobiolaging.2017.06.018.
36. Arai T, Hasegawa M, Akiyama H, Ikeda K, Nonaka T, Mori H, Mann D, Tsuchiya K, Yoshida M, Hashizume Y, Oda T. TDP-43 is a component of ubiquitin-positive tau-negative inclusions in frontotemporal lobar degeneration and amyotrophic lateral sclerosis. Biochem Biophys Res

Commun. 2006;351(3):602–11. Epub 2006/11/07. doi: 10.1016/j.bbrc.2006.10.093. [PubMed: 17084815]

37. Neumann M Molecular neuropathology of TDP-43 proteinopathies. International journal of molecular sciences. 2009;10(1):232–46. doi: 10.3390/ijms10010232.; [PubMed: 19333444]
38. Neumann M, Sampathu DM, Kwong LK, Truax AC, Micsenyi MC, Chou TT, Bruce J, Schuck T, Grossman M, Clark CM, McCluskey LF, Miller BL, Masliah E, Mackenzie IR, Feldman H, Feiden W, Kretzschmar HA, Trojanowski JQ, Lee VM. Ubiquitinated TDP-43 in frontotemporal lobar degeneration and amyotrophic lateral sclerosis. Science. 2006;314(5796):130–3. Epub 2006/10/07. doi: 10.1126/science.1134108. [PubMed: 17023659]
39. Barmada SJ, Skibinski G, Korb E, Rao EJ, Wu JY, Finkbeiner S. Cytoplasmic mislocalization of TDP-43 is toxic to neurons and enhanced by a mutation associated with familial amyotrophic lateral sclerosis. The Journal of neuroscience : the official journal of the Society for Neuroscience. 2010;30(2):639–49. doi: 10.1523/JNEUROSCI.4988-09.2010.;
40. Hasegawa M, Arai T, Nonaka T, Kametani F, Yoshida M, Hashizume Y, Beach TG, Buratti E, Baralle F, Morita M, Nakano I, Oda T, Tsuchiya K, Akiyama H. Phosphorylated TDP-43 in frontotemporal lobar degeneration and amyotrophic lateral sclerosis. Annals of neurology. 2008;64(1):60–70. Epub 2008/06/12. doi: 10.1002/ana.21425.; [PubMed: 18546284]
41. Mori F, Tanji K, Odagiri S, Toyoshima Y, Yoshida M, Kakita A, Takahashi H, Wakabayashi K. Autophagy-related proteins (p62, NBR1 and LC3) in intranuclear inclusions in neurodegenerative diseases. Neuroscience letters. 2012;522(2):134–8. Epub 2012/06/26. doi: 10.1016/j.neulet.2012.06.026. [PubMed: 22728060]
42. Zatloukal K, Stumptner C, Fuchsbichler A, Heid H, Schnoelzer M, Kenner L, Kleinert R, Prinz M, Aguzzi A, Denk H. p62 Is a common component of cytoplasmic inclusions in protein aggregation diseases. The American journal of pathology. 2002;160(1):255–63. Epub 2002/01/12. doi: 10.1016/S0002-9440(10)64369-6.; [PubMed: 11786419]
43. Alves-Rodrigues A, Gregori L, Figueiredo-Pereira ME. Ubiquitin, cellular inclusions and their role in neurodegeneration. Trends in neurosciences. 1998;21(12):516–20. Epub 1999/01/09. doi: 10.1016/s0166-2236(98)01276-4. [PubMed: 9881849]
44. Li L, Wang ZV, Hill JA, Lin F. New autophagy reporter mice reveal dynamics of proximal tubular autophagy. Journal of the American Society of Nephrology : JASN. 2014;25(2):305–15. doi: 10.1681/ASN.2013040374.; [PubMed: 24179166]
45. Vorhees CV, Williams MT. Morris water maze: procedures for assessing spatial and related forms of learning and memory. Nature protocols. 2006;1(2):848–58. Epub 2007/04/05. doi: 10.1038/nprot.2006.116.; [PubMed: 17406317]
46. Cazares VA, Rodriguez G, Parent R, Ouillette L, Glanowska KM, Moore SJ, Murphy GG. Environmental variables that ameliorate extinction learning deficits in the 129S1/SvlmJ mouse strain. Genes Brain Behav. 2019;18(7):e12575 Epub 2019/04/12. doi: 10.1111/gbb.12575.; [PubMed: 30973205]
47. McKinney BC, Sze W, White JA, Murphy GG. L-type voltage-gated calcium channels in conditioned fear: a genetic and pharmacological analysis. Learning & memory. 2008;15(5):326–34. Epub 2008/04/29. doi: 10.1101/lm.893808.; [PubMed: 18441291]
48. Temme SJ, Murphy GG. The L-type voltage-gated calcium channel CaV1.2 mediates fear extinction and modulates synaptic tone in the lateral amygdala. Learning & memory. 2017;24(11):580–8. Epub 2017/10/19. doi: 10.1101/lm.045773.117.; [PubMed: 29038219]
49. Wotjak CT. Sound check, stage design and screen plot - how to increase the comparability of fear conditioning and fear extinction experiments. Psychopharmacology (Berl). 2019;236(1):33–48. Epub 2018/11/25. doi: 10.1007/s00213-018-5111-5.; [PubMed: 30470861]
50. Phillips RG, LeDoux JE. Differential contribution of amygdala and hippocampus to cued and contextual fear conditioning. Behavioral neuroscience. 1992;106(2):274–85. Epub 1992/04/01. doi: 10.1037//0735-7044.106.2.274. [PubMed: 1590953]
51. Pearring JN, Salinas RY, Baker SA, Arshavsky VY. Protein sorting, targeting and trafficking in photoreceptor cells. Prog Retin Eye Res. 2013;36:24–51. Epub 2013/04/09. doi: 10.1016/j.preteyeres.2013.03.002.; [PubMed: 23562855]

52. Young RW. The renewal of photoreceptor cell outer segments. The Journal of cell biology. 1967;33(1):61–72. Epub 1967/04/01. doi: 10.1083/jcb.33.1.61.; [PubMed: 6033942]

53. Mann JR, Gleixner AM, Mauna JC, Gomes E, DeChellis-Marks MR, Needham PG, Copley KE, Hurtle B, Portz B, Pyles NJ, Guo L, Calder CB, Wills ZP, Pandey UB, Kofler JK, Brodsky JL, Thathiah A, Shorter J, Donnelly CJ. RNA Binding Antagonizes Neurotoxic Phase Transitions of TDP-43. Neuron. 2019;102(2):321–38 e8. Epub 2019/03/04. doi: 10.1016/j.neuron.2019.01.048.; [PubMed: 30826182]

54. Gasset-Rosa F, Lu S, Yu H, Chen C, Melamed Z, Guo L, Shorter J, Da Cruz S, Cleveland DW. Cytoplasmic TDP-43 De-mixing Independent of Stress Granules Drives Inhibition of Nuclear Import, Loss of Nuclear TDP-43, and Cell Death. Neuron. 2019;102(2):339–57 e7. Epub 2019/03/12. doi: 10.1016/j.neuron.2019.02.038.; [PubMed: 30853299]

55. Frottin F, Schueder F, Tiwary S, Gupta R, Korner R, Schlichthaerle T, Cox J, Jungmann R, Hartl FU, Hipp MS. The nucleolus functions as a phase-separated protein quality control compartment. Science. 2019;365(6451):342–7. Epub 2019/07/13. doi: 10.1126/science.aaw9157. [PubMed: 31296649]

56. Mediani L, Guillen-Boixet J, Vinet J, Franzmann TM, Bigi I, Mateju D, Carra AD, Morelli FF, Tiago T, Poser I, Alberti S, Carra S. Defective ribosomal products challenge nuclear function by impairing nuclear condensate dynamics and immobilizing ubiquitin. The EMBO journal. 2019;38(15):e101341 Epub 2019/07/05. doi: 10.15252/embj.2018101341.; [PubMed: 31271238]

57. Wu Q, Liu M, Huang C, Liu X, Huang B, Li N, Zhou H, Xia XG. Pathogenic Ubqln2 gains toxic properties to induce neuron death. Acta neuropathologica. 2015;129(3):417–28. doi: 10.1007/s00401-014-1367-y. [PubMed: 25388785]

58. Yao J, Qiu Y, Frontera E, Jia L, Khan NW, Klionsky DJ, Ferguson TA, Thompson DA, Zacks DN. Inhibiting autophagy reduces retinal degeneration caused by protein misfolding. Autophagy. 2018;14(7):1226–38. Epub 2018/06/27. doi: 10.1080/15548627.2018.1463121.; [PubMed: 29940785]

59. Lobanova ES, Finkelstein S, Li J, Travis AM, Hao Y, Klingeborn M, Skiba NP, Deshaies RJ, Arshavsky VY. Increased proteasomal activity supports photoreceptor survival in inherited retinal degeneration. Nature communications. 2018;9(1):1738 Epub 2018/05/02. doi: 10.1038/s41467-018-04117-8.;

60. Kosmaoglou M, Schwarz N, Bett JS, Cheetham ME. Molecular chaperones and photoreceptor function. Prog Retin Eye Res. 2008;27(4):434–49. Epub 2008/05/21. doi: 10.1016/j.preteyeres.2008.03.001.; [PubMed: 18490186]

61. Lobanova ES, Finkelstein S, Skiba NP, Arshavsky VY. Proteasome overload is a common stress factor in multiple forms of inherited retinal degeneration. Proceedings of the National Academy of Sciences of the United States of America. 2013;110(24):9986–91. Epub 2013/05/30. doi: 10.1073/pnas.1305521110.; [PubMed: 23716657]

Highlights NBD-20–248

- *In vivo* aggregation of mutant UBQLN2 is insufficient to cause neurodegeneration.
- Intraneuronal inclusions of WT UBQLN2 support the theory of UBQLN2 LLPS *in vivo*.
- Overexpression of UBQLN2 results in dose-dependent decrease in HSP70.
- Overexpression of UBQLN2 results in dose-dependent retinal degeneration.
- Altering levels of UBQLN2 may have deleterious effects on protein homeostasis.

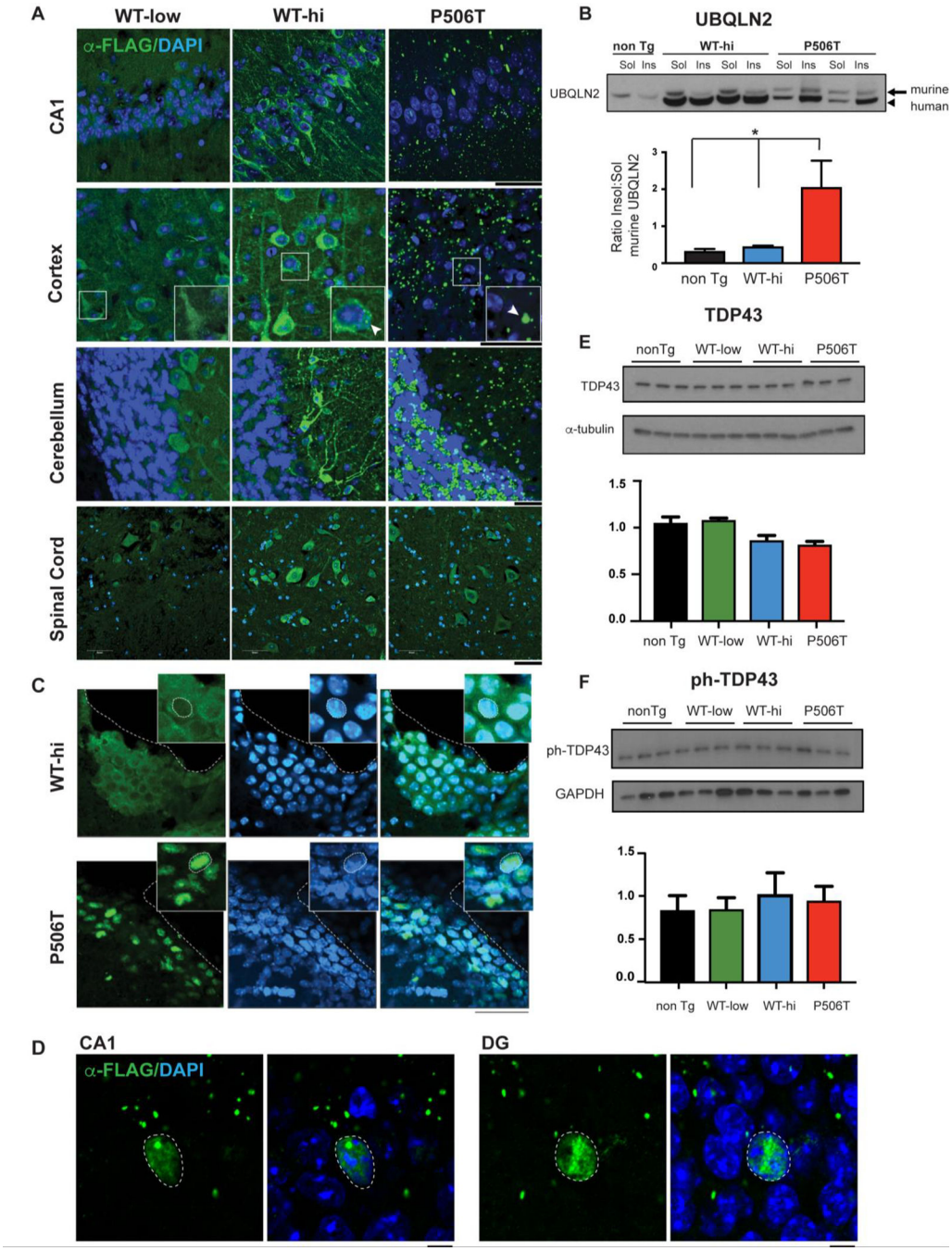

Figure 1. WT and mutant (P506T) UBQLN2 differ in aggregation and subcellular localization in transgenic mouse brain.

A. Transgenic WT-UBQLN2 is largely diffusely located in neurons while P506T-UBQLN2 aggregates robustly across essentially all brain regions. Representative immunofluorescence in major brain regions from 3 transgenic mouse lines (3 months old) expressing FLAG-tagged WT- or P506T-UBQLN2 under control of the mouse prion promoter. Tissue sections were stained for transgenic FLAG-tagged UBQLN2 (green) and DAPI (blue). Magnified (2x) insets in cortex panel highlight punctate UBQLN2 staining. Arrows indicate puncta present in WT-hi and P506T mice that are absent in WT-low mice. Scale bars: 50 μm.

B. Mutant UBQLN2 sequesters endogenous murine UBQLN2 into the insoluble fraction. Representative Western blot of soluble and insoluble brain fractions from transgenic (two mice) and non-transgenic mice (1 mouse) probed with anti-UBQLN2 antibody. Murine UBQLN2 (arrow) and transgenic human UBQLN2 (arrow head) can be distinguished by size. The insoluble fraction of murine UBQLN2 is significantly increased in mice expressing mutant, but not WT, transgenic UBQLN2. In three independent experiments, the average insoluble/soluble ratio for murine UBQLN2 was quantified from relative band intensities (* = $P < 0.05$. Error bars = SEM).

C. Mutant, but not WT, UBQLN2 in transgenic mice localizes to nuclei in neuroendothelial cells. Immunofluorescence in the lateral ventricle from WT-hi and P506T mice stained for FLAG-UBQLN2 (green) and DAPI (blue) shows WT-UBQLN2 is largely cytoplasmic whereas P506T-UBQLN2 co-localizes to nuclei (coincident with DAPI). Dotted white lines outline the ventricle edge and cell nuclei (inset). Sections are from 6 month old mice. Scale bars: 50 μm.

D. P506T-UBQLN2 occasionally translocates to the nuclei of neurons in the hippocampus of transgenic mice. Immunofluorescence of the CA1 and dentate gyrus (DG) from P506T mice stained for FLAGU-BQLN2 (green) and DAPI (blue) shows P506T-UBQLN2 co-localized to nuclei (coincident with DAPI). Dotted white lines outline the cell nuclei. Scale bars: 5 μm.

E,F. TDP43 and phospho-TDP43 levels are not significantly changed in brain lysates from UBQLN2 transgenic mice.

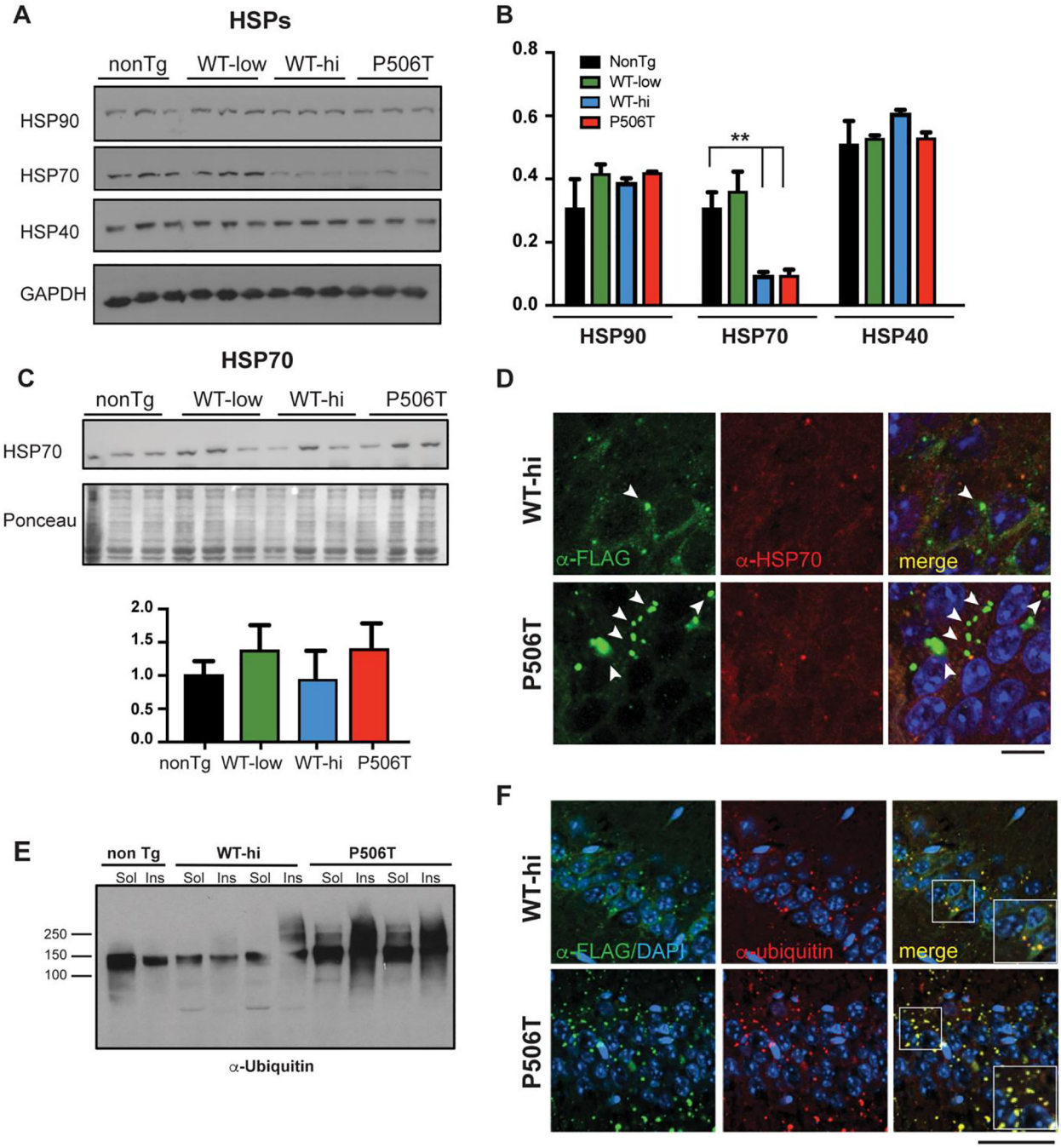

Figure 2. WT- and P506T-UBQLN2 induce changes in key protein quality control markers

A, B. By Western blot analysis (A), HSP70 levels are significantly decreased in WT-hi and P506T mice while two other chaperones, HSP40 and HSP90, remain unchanged. Relative band intensities were quantified and graphed (B). ** = P< 0.01, error bars = ± SEM.

C. HSP70 levels are not elevated in the insoluble fraction of brain lysates from WT-hi and P506T mice on Western blot. Pellets from RIPA lysates of brain tissue were solubilized in 3X SDS sample buffer and analyzed by Western blot. Relative band intensities were quantified after normalization to Ponceau loading control and graphed.

D. Representative immunofluorescence tissue sections from the CA1 of WT-hi and P506T mice stained for transgenic FLAG-tagged UBQLN2 (green), HSP70 (red) and DAPI (blue). Arrows indicate occasional colocalization of HSP70 with small UBQLN2 positive puncta. Note that larger UBQLN2 aggregates (white arrows) are negative for HSP70 and occur more frequently in P506T mice. Scale bars: 10 μm.

E. Western blot of soluble and insoluble brain lysate fractions from transgenic and non-transgenic mice, probed with anti-ubiquitin antibody.

F. Co-immunofluorescence with antibodies detecting transgenic UBQLN2 (anti-FLAG, green) and ubiquitin (red) in the CA1 region of the hippocampus show that both UBQLN2 puncta (WT-hi mice) and aggregates (P506T mice) strongly co-localize with ubiquitin. Magnified (1.5x) insets in the merged panels highlight the colocalization of the staining (yellow). Scale bar: 50 μm.

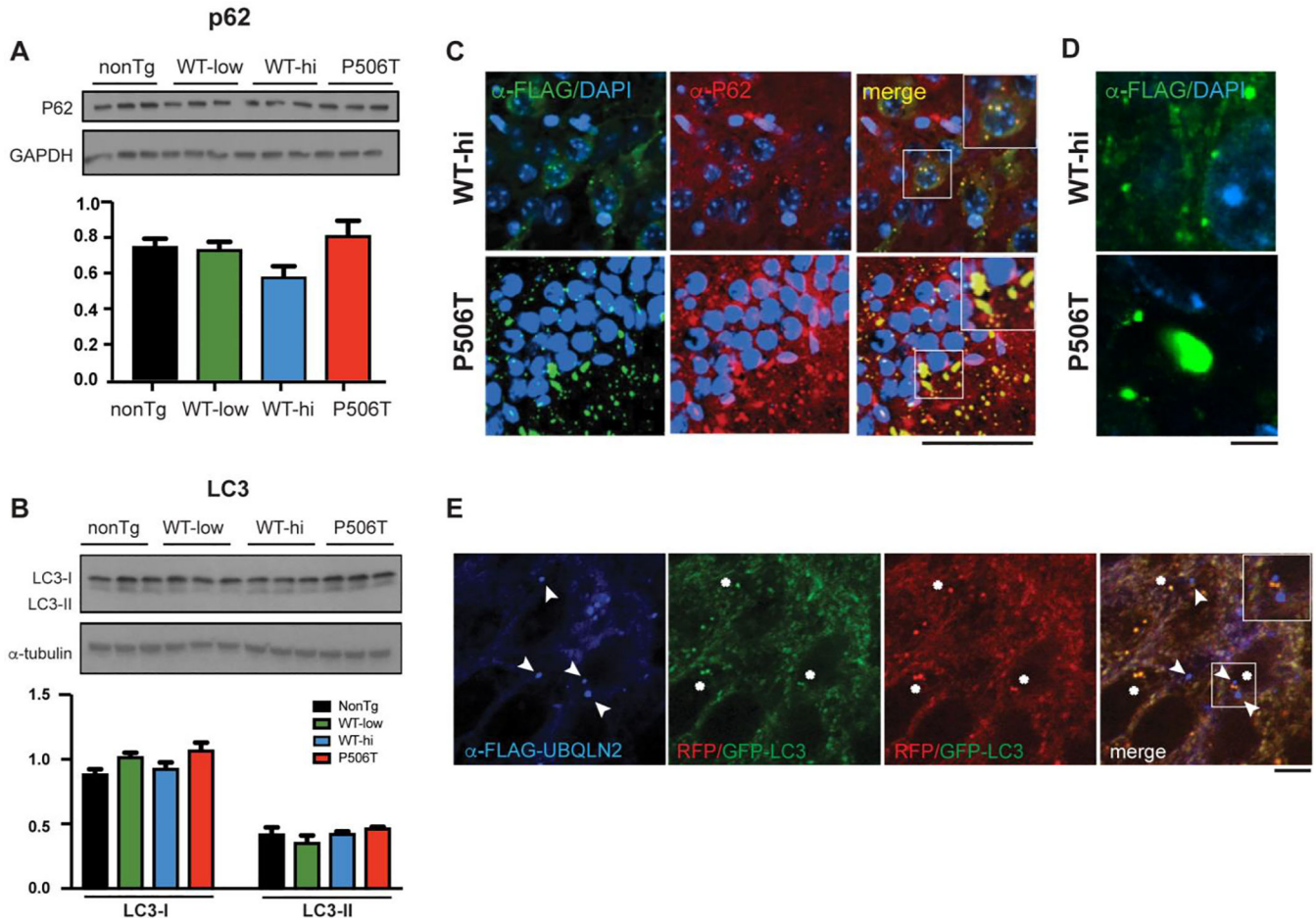

Figure 3. WT and P506T puncta colocalize with P62 but not LC3

A. Western blot analysis of brain lysates shows no changes in p62 in UBQLN2 transgenic mouse lines (WT-low, WT-hi and P506T) compared to nonTg mice (6 months old).

B. Western blot analysis of brain lysates shows no changes in the autophagy marker LC3 in UBQLN2 transgenic mouse lines (WT-low, WT-hi and P506T) compared to nonTg mice (6 months old).

C. Co-immunofluorescence with antibodies detecting transgenic UBQLN2 (anti-FLAG, green) and p62 (red) in the CA1 region of the hippocampus show that smaller UBQLN2 puncta in WT-hi mice and larger aggregates in P506T mice both co-localize with p62. Magnified (1.5x) insets in merged panels highlight the colocalization of the staining (yellow). Scale bar: 50μm.

D. High magnification view of UBQLN2 puncta in WT-hi and P506T mice in the CA1 region. Scale bar: 5μm.

E. LC3, an autophagosome marker, does not co-localize with WT-UBQLN2 puncta. Hippocampal tissue sections from WT-hi mice that had been crossed to GFP/RFP-LC3 transgenic mice were immunostained for FLAG-UBQLN2. UBQLN2 puncta (blue, signified with arrowheads) are distinct from GFP/RFP autophagosomes (red or green; yellow in merged image, signified with asterisks). The magnified (1.5x) inset in the merged panel

highlights the distinction between the autophagosomes (yellow) and the UBQLN2 puncta (blue). Scale bar 5μm.

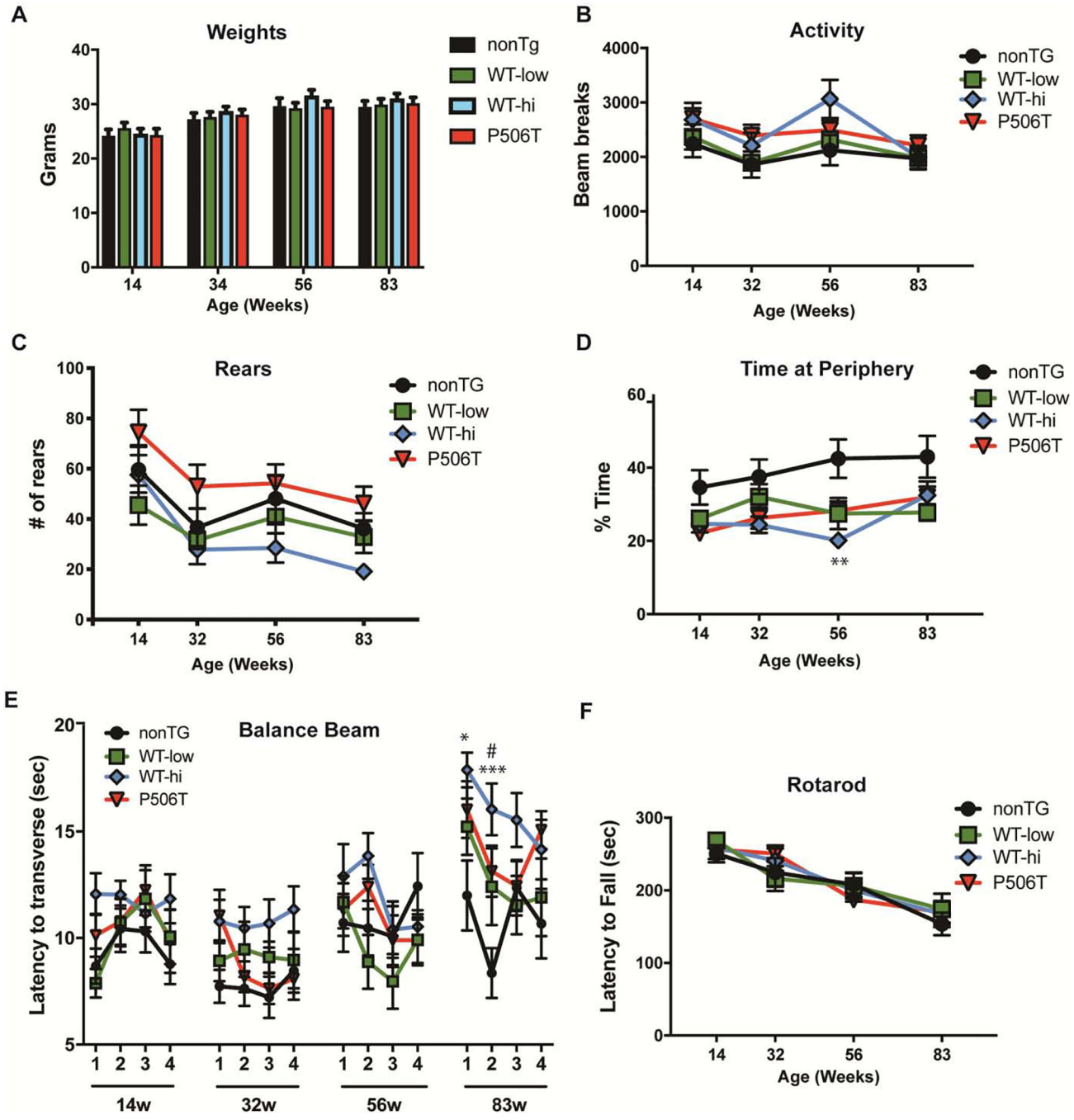

Figure 4. Phenotypic evaluation reveals limited changes in transgenic mice expressing WT or mutant UBQLN.

A. All transgenic mice show normal weights over time compared to control mice.

B, C. Exploratory activity on open-field test is unchanged in transgenic mice. Total activity levels assessed by the number of beam breaks (B) and rearing behavior (C) did not significantly differ between nonTG and UBQLN2 mice.

D. Transgenic mice do not display anxiety-like behavior, assessed by the percentage of time spent on the open field periphery. A significant difference (** = P <.01) noted in WT-hi mice at 56 weeks compared to nonTG mice was not present at other time points.

E. WT-hi and P506T mice show a slight deficit in 5-mm beam walking test at 83 weeks, determined by measuring the time to traverse the beam compared to nonTg mice. Data points represent mean time to traverse the beam per trial/day/week ± SEM). * = P<0.05, WT-hi; *** = P<0.001, WT-hi; # = P<0.05, P506T.

F. No motor impairment was detected by accelerating rotarod. Latency to fall during the 5 min test was measured, and data points represent the mean of the better of two trails on each testing day, ± SEM.

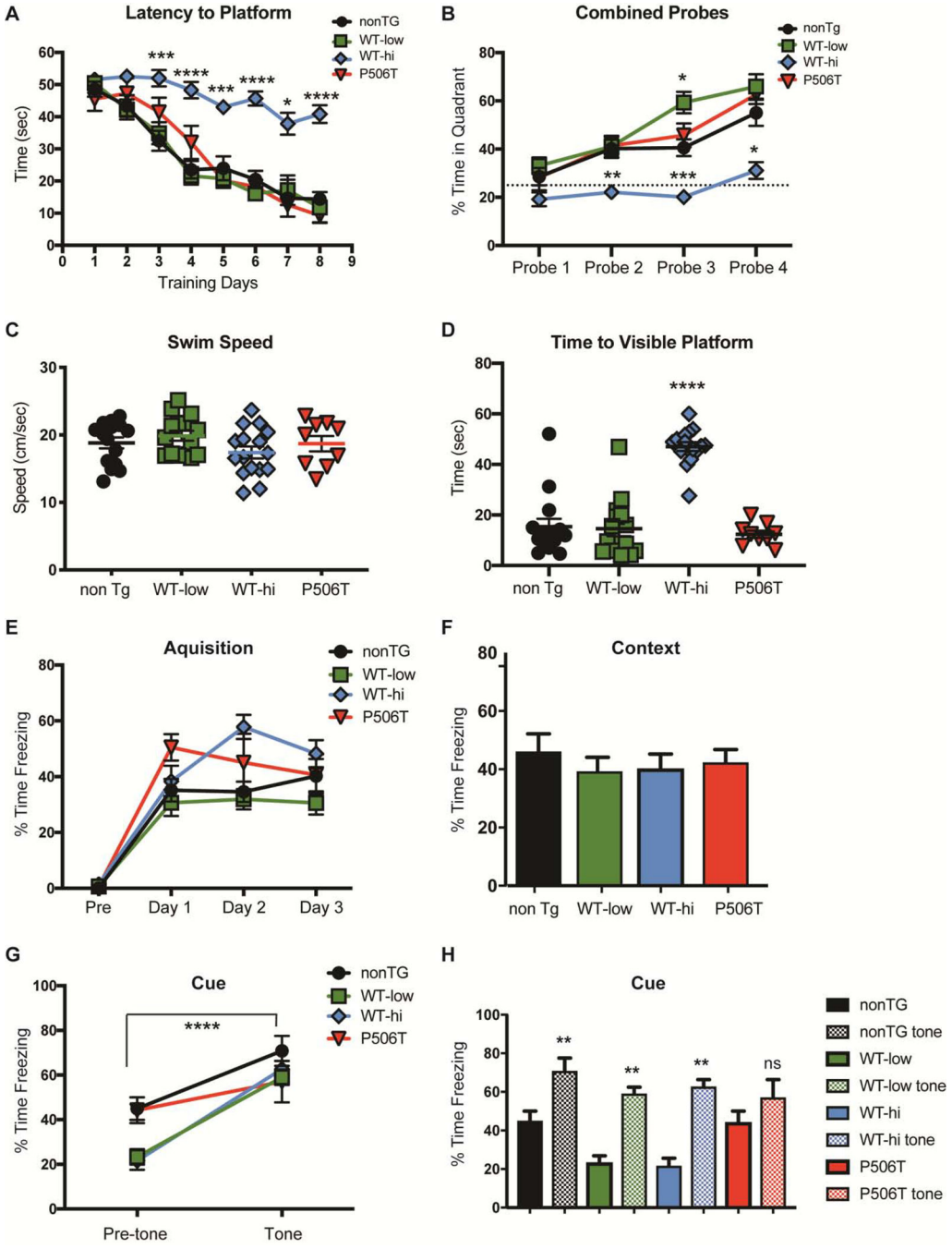

Figure 5. WT-hi mice are significantly impaired in the Morris water maze, but fear conditioning is not altered in WT- or P506T-UBQLN2 transgenic mice.

A. Time to reach the hidden platform (latency) was significantly increased in WT-hi mice compared to all other genotypes. Mice were trained for six trials a day for 8 d.

B. In 60-sec probe trials 2–4 (indicated by black arrows in panel A) only WT-hi mice failed to spend more time in the quadrant where the platform was previously located (Q4). The dashed line (25%) represents random or "chance" performance.

C. Swim speeds were unchanged among transgenic mice compared in nonTG mice.

D. Average escape latencies for WT-low and P506T mice recorded during the visible platform version of the Morris water maze. WT-hi mice escape latencies were markedly increased over all other genotypes suggesting an impairment in finding the marked platform, which is independent of hippocampal function.

E. Mice were fear-conditioned with three tone-footshock pairings per day for 3 d. Similar increases in percent time freezing over the days of training show normal acquisition in all mice.

F. 24 hr after the last training day, mice were tested for their contextual fear memory. Mice of all genotypes exhibited a similar increase in freezing to the context as nonTg mice.

G, H. 24 hr after the context test, mice were tested for cued fear memory. Mice were placed in a novel environment and exposed to the tone alone. WT-low and WT-hi displayed a significant increase infreezing similar to nonTg mice, whereas P506T mice did not show statistically increased freezing. Bar graph representations of changes in post- versus pre-tone freezing are shown in H.

For all graphs * = $P > 0.05$, ** = $P > 0.01$, *** = $P<0.001$, **** = $P<0.0001$. Error bars = ± SEM.

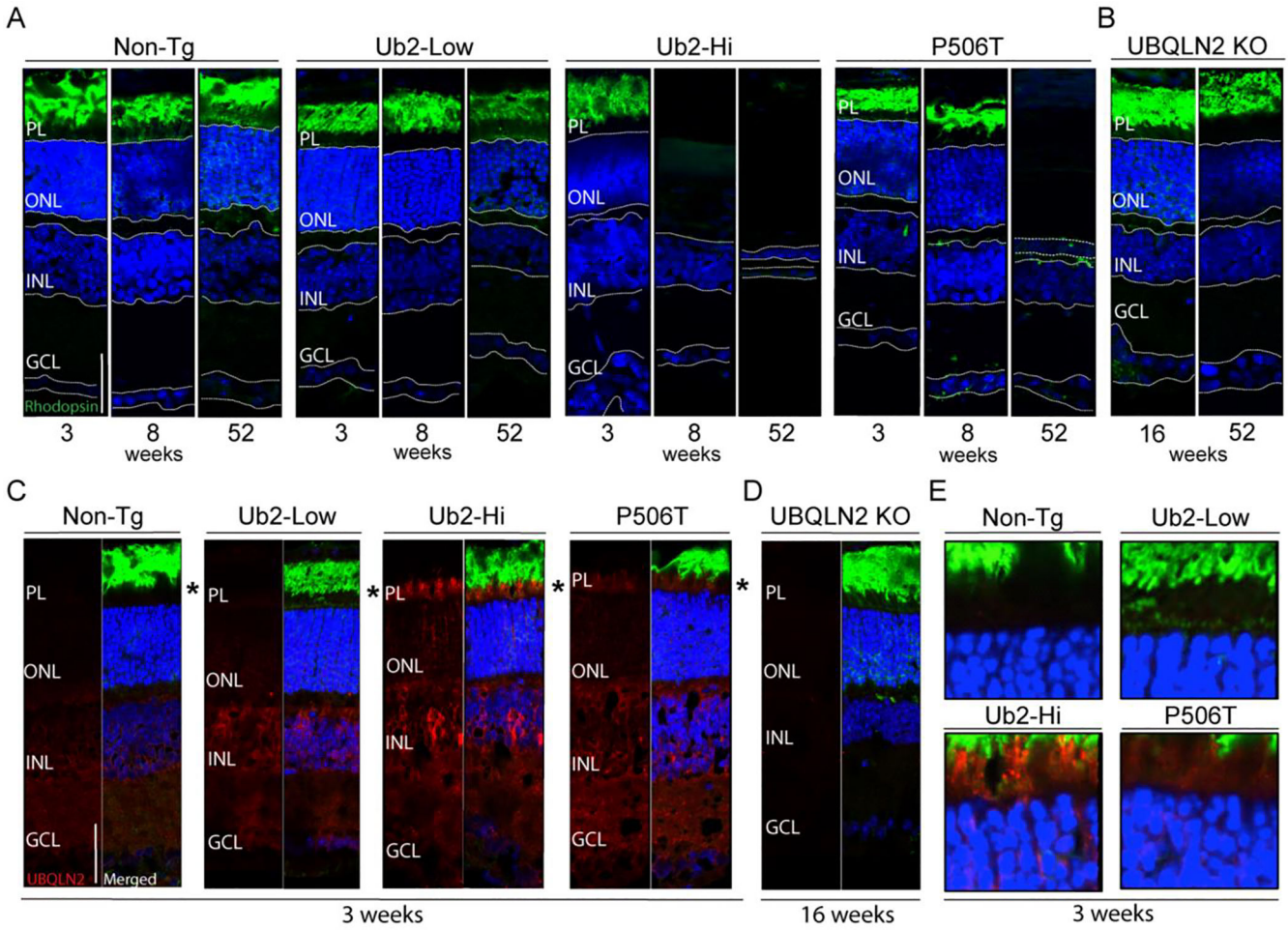

Figure 6. Overexpression of UBQLN2 results in dose-dependent retinal degeneration.

A. All retinal layers are present in non-transgenic and WT-low mice at 3, 8 and 52 weeks of age (n=4–6). PL=Photoreceptor layer, ONL=Outer Nuclear Layer, INL=Inner Nuclear Layer, GCL=Ganglion Cell layer). WT-Hi mice show all retinal layers at 3 weeks of age but by 8 weeks of age, the PL and ONL are absent (n=4–6). P506T mice display all retinal layers at 3 and 8 weeks of age but show a complete loss of the PL and significant loss of ONL at 52 weeks (n=4).

B. UBQLN2 KO mice display no retinal degeneration up to 52 weeks of age (n=3).

C. UBQLN2 expression at 3 weeks. Non-Tg animals display low and diffuse endogenous UBQLN2 expression in the retina, largely in the INL and GCL (n=5). WT-Low mice show diffuse expression of UBQLN2 throughout the retina, with pronounced expression in the INL and GCL (n=5). WT-Hi mice show robust, punctate expression of UBQLN2 throughout the retina (n=4). P506T mice show robust expression of UBQLN2 throughout the retina with some punctate expression (n=4).

D. UBQLN2 KO mice show no reactivity with UBQLN2 antibody (n=3). Scale bar= 50uM

E. Enlarged view of regions signified by asterisks in C.